Electron-Capture Decays mimicking Axionic Transitions

Master's Thesis, 15.05.2024

Author:

Aagrah Agnihotri

Supervisor:

Prof. Jouni Suhonen

UNIVERSITY OF JYVÄSKYLÄ
DEPARTMENT OF PHYSICS

Abstract

For the first time, estimates for β decay rates are made that are necessary for experimental searches of low-mass axions. Low-mass axions are potential dark matter candidates, hence, searches of low-mass axions have implications beyond standard model physics. For terrestrial searches of low-mass axions, ^{44}Ti, ^{57}Co, and ^{139}Ce are popular sources. The sources decay purely via electron-capture and populate M1-decaying excited states in daughter nuclei. These M1-decaying nuclear-excited states are also expected to decay via axion production. The GS-to-GS branches of the electron-capture decays of ^{44}Ti, ^{57}Co, and ^{139}Ce, not yet measured are expected to have identical experimental signatures as the axionic transitions. These GS-to-GS transitions are rare, and experiments call for theory predictions for transition rates of these decay branches. The scope of the work done addresses such needs of the experiments.

Aagrah Agnihotri
Monograph
Master's thesis
Department of Physics, University of Jyväskylä, 2024, 39 pages.

Keywords: electron-capture decays, axion, dark matter

Tiivistelmä

Tässä työssä tehdään ensimmäistä kertaa arviot beetahajoamisnopeuksista, jotka ovat välttämättömiä keveitä aksioneja etsivien kokeiden kannalta. Keveät aksionit ovat potentiaalisia ehdokkaita pimeäksi aineeksi, joten niiden etsinnöillä on vaikutuksia standardimallin ulkopuolisen fysiikan löytymisen mahdollisiin. Keveiden aksionien kokeellisissa etsinnöissä 44Ti, 57Co ja 139Ce ovat suosittuja beetalähteitä. Nämä lähteet hajoavasti puhtaasti elecktronin sieppauksen kautta ja syöttävät tytärytimien M1 (magneettinen dipoli)-hajoavia viritystiloja. Näiden M1-hajoavien viritystilojen arvellaan purkautuvan myös aksionituoton kautta. Toisaalta 44Ti:n, 57Co:n ja 139Ce:n perustilalta perustilalle tapahtuvat electronisieppaushajoamiset tuottavat oletetusti samanlaisen kokeellisen signaalin kuin aksioniset siirtymät. Nämä perustilalta perustilalle tapahtuvat siirtymät ovat hyvin harvinaisia eikä niitä ole vielä pystytty mittaamaan, joten kokeet hyötyvät näiden hajoamisten siirtymänopeuksien teoriaennusteista. Tätä kautta tässä työssä tehty tutkimus pyrkii helpottamaan aksionimittausten haasteita.

Aagrah Agnihotri
Monografia
Pro gradu -tutkielma
Fysiikan laitos, Jyväskylän yliopisto, 2024, 39 sivua

Avainsanat: elektronisieppaus, aksioni, pimeä aine

Acknowledgements

...to the soft and still voice that called me to pursue physics, truth, beauty, meaning, and purpose thereof, to go on the adventure of my life...I am eternally grateful.

I start by expressing the deep gratitude I feel for having Prof. Jouni Suhonen as my teacher and supervisor. I started my research at the University of Jyväskylä in March 2023 under his guidance, and words cannot express how enriching and meaningful experience it has been to learn from him. His boundless enthusiasm for physics, his capacity to engage in research in a wide range of topics, and his generosity of ideas and resources toward his students and collaborators are awe-inspiring. I feel truly blessed that I met him and got the opportunity to work with him at a pivotal moment in my career and studies.

I have lost count of people who have helped me, in crucial ways so that I could pursue my dream of becoming a physicist. I thank everyone I met inside and outside the faculty of mathematics and science, who helped me along my journey. I am especially thankful for having friends who have helped me and have accompanied me as we pursued our journeys. I am grateful to them for being a constant and wonderful presence in my life.

Last but not least, I thank my family for all the sacrifices they made, to provide me with all the opportunities I received in this life. I thank especially, my grandparents for they raised me.

To my grandmother who passed away this year, I want to say that I miss you dearly. Thank you for everything Dadi.

Aagrah Agnihotri
Jyväskylä May 07, 2024

Preface

Investigation of physical phenomena that are divorced from the domain of human perception, involves full engagement of the human capacity to abstract, imagine, and create. Limitations of perception are overcome through ingenuity and invention. The study of nuclear dynamics and processes being one such endeavor, is a challenging and rewarding enterprise.

The study of nuclear β decays has important implications for Beyond Standard Model Physics (BSMP) [1–5]. Among different avenues of searches for BSMP, where the study of nuclear β decays plays an important role, experimental searches for low-mass axions are among such avenues [6, 7]. The experiments involved in the searches of low-mass axions, call for theory to make predictions for presently unknown electron-capture transitions relevant to experimental searches of such axions. This work aims to fulfill such needs.

The author hopes that this work conveys the excitement and joy the author felt while being engaged in the project that led to the making of this work.

Jyväskylä May 7, 2024

Aagrah Agnihotri

Contents

1 Introduction

Axions are hypothesized Goldstone pseudoscalar bosons, that were proposed as a solution to the strong CP problem in 1977-78 [8–10]. Low-mass axions are also potential dark matter candidates [11]. Such implications for Beyond Standard Model Physics (BSMP), motivate the experimental searches of axions. Axions can be produced via decays of M1-decaying nuclear-excited states. This is so since axions are similar to magnetic dipole photons in their pseudoscalar character, and can couple to nucleons [12]. Therefore, the possibility of using strong radioactive sources for terrestrial searches of low-mass axions becomes real [6, 7]. ^{44}Ti, ^{57}Co, and ^{139}Ce are among the popular sources that can be used for terrestrial searches of low-mass axions.

^{44}Ti, ^{57}Co, and ^{139}Ce decay purely via electron-capture (EC) decay. The M1-decaying excited states ^{44}Sc*(0_1^-), ^{57}Fe*$(3/2_1^-)$, and ^{139}La*$(5/2_1^+)$ are populated directly or indirectly in the respective electron-capture decays. The known electron-capture branches for the three sources include allowed Gamow-Teller (GT) transitions ^{57}Co$(7/2_1^-) \rightarrow ^{57}$Fe*$(5/2_1^-)$, ^{57}Co$(7/2_1^-) \rightarrow ^{57}$Fe*$(5/2_2^-)$, and ^{139}Ce$(3/2_1^+) \rightarrow ^{139}$La*$(5/2_1^+)$, along with 1$^{\text{st}}$ forbidden non-unique transitions ^{44}Ti$(0_1^+) \rightarrow ^{44}$Sc*$(1_1^-)$ and ^{44}Ti$(0_1^+) \rightarrow$ ^{44}Sc*(0_1^-).

In addition to these known branches, there exists a real possibility of ground state-to-ground state (GS-to-GS) transitions, including 2$^{\text{nd}}$-forbidden non-unique decays: ^{44}Ti$(0_1^+) \rightarrow ^{44}Sc(2_1^+)$ and ^{139}Ce$(3/2_1^+) \rightarrow ^{139}La(7/2_1^+)$, along with the 2$^{\text{nd}}$ forbidden unique decay ^{57}Co$(7/2_1^-) \rightarrow ^{57}Fe(1/2_1^-)$. The experimental branching ratios (BRs) for these GS-to-GS transitions are unknown. The reason for this is the strong suppression of GS-to-GS transition in the presence of alternate less hindered electron-capture branches. This causes the electron-capture decaying parent sources to decay almost entirely via the present known branches.

Experimental determination of these GS-to-GS branching ratios is necessary for the experimental confirmation of the event of axion production. This is so because GS-to-GS transitions can mimic the potential event of axion production in experiments. The experimental signatures for both events are X-rays and Auger electrons from

the electron-capture decays [6]. Therefore, experiments call for theoretical estimates of branching ratios for the GS-to-GS branches as a guide. To serve such needs of the experiments is the focus of this work.

Nuclear structure calculations in the framework nuclear shell model are done to predict transition rates of GS-to-GS forbidden electron-capture decays. Advanced theory of β decay is used to evaluate the physics of these forbidden electron-capture decays. Key aspects of the phenomenology of g_A quenching are drawn upon, due to their importance in the theoretical study of all weak interaction nuclear processes including β decays.

In the sections ahead, a pedagogical presentation of the foundations and framework of the nuclear shell model will be made along with the theory of β decay. The phenomenology of g_A quenching is discussed in the light of the present work.

2 Theoretical background

2.1 Nuclear Shell Model

2.1.1 Foundations

Nuclei can be aptly characterized as nuclear many-body bound systems of hadrons. In nuclear phenomenology, among the practical treatments of such systems, protons and neutrons (together referred to as nucleons) are viewed to generate the potential that holds them in bound states. This potential due to strong nuclear interaction between nucleons, can be modeled phenomenologically [13]. Also, Hartree-Fock method [13–15] and Brueckner Hartree-Fock (BHF) method [14, 15] offer an iterative procedure to obtain realistic self-consistent nuclear potentials. Hartree-Fock method derives the single-particle potential using potential, whereas BHF uses G-matrix to do the same [14, 15]. Details of the mathematical treatment of these methods, and, a tour de force of nuclear interaction physics in relation to the nuclear many-body problem can be found in Refs. [14, 15].

Among the successful nuclear models to date, the nuclear shell model is in a class of its own. The modern versions of the shell model, namely, the Monte Carlo and No-Core Shell Models, augmented with advances in nuclear theory and many-body methods are among state-of-the-art treatments of the nuclear many-body systems [16]. Even with large computational capabilities, full-scale shell model calculations remain out of reach for most nuclei. The standard nuclear shell model stands today as the most practical and commonly used version of the shell model. The standard shell model involves the treatment of a nucleus consisting of a core, with valence nucleons moving in an empirically fitted mean field and interacting via empirically fitted effective two-body residual interactions [13–15, 17–19].

There are several assumptions in such a picture of nuclear structure dynamics. The success of the nuclear shell model, speaks to the physical relevance of such assumptions. We briefly outline the key assumptions that speak to different aspects of the physics of nuclei.

The totality of the nucleon interactions acting within nuclei is summed up for the most part as giving rise to effectively mean-field-like dynamics. This effect manifests as the almost independent movement of the nucleons in the nuclear medium. The seemingly independent motion is caused when repulsive components of the nucleon interactions almost balance the attractive components. The repulsive components include the short-range repulsive component of the nucleon-nucleon (NN) interactions, the Pauli principle, tensor force contributions, and the repulsive potential between nucleons occupying relative P states. These effects almost balance out the totality of the attractive components of the NN interaction, such as attraction between nucleons in S states. This also explains the mostly constant nuclear density for all nuclei [14].

The independent particle picture of nucleons moving in a mean field leads to the observed nuclear shell structure. We denote the Hamiltonian of such picture as $H_0 = \sum[T_i + U_i]$. Here T_i and U_i represent the kinetic and mean field potential energies. The nucleons are viewed as occupying single-particle states in the mean field, and nuclear many-body wave functions are the Slater determinants of the single-particle states. The Schrodinger equation is further simplified by treating the system of N nucleons as one consisting of a core and valence nucleons in a truncated valence space. This simplification works due to pairing aspects of the NN interaction [13, 14, 17–19].

Since the nucleon movement is not entirely independent in the nuclear medium, the residual interaction V is incorporated to give a more accurate description of nuclear dynamics. The final Hamiltonian is given as $H = H_o + V$, where the perturbative treatment of residual interaction is due to its relative weakness in comparison to the mean field potential U_i. V is designed to account for the core polarization effect of valence nucleons, the interaction of core and valence nucleons, and interactions among the valence nucleons. The effective V is tuned such that solutions of the shell model Hamiltonian H, form a subset of solutions of the interacting N-body system. V can mix the configurations (Slater determinants) emerging as the solutions/eigenfunctions of the Hamiltonian H_0, the wave functions generated due to such mixing are the eigenfunctions of Hamiltonian H [14].

The shell model works best for nuclei at or near shell closures, shell closures being configurations of N and Z where the given set of orbitals are completely filled. Such configurations can define the core beyond which lie the nucleons in the active valence space.

For most Hamiltonians in use, V is treated as the sum of two-body interactions among individual nucleons. Today there are Hamiltonians that are equipped with even three-body interactions. Two-body residual interactions that incorporate only two-body correlations work, because they dominate three-body and higher many-body correlations. This justifies that including higher many-body correlations improves the quality of the predictions asymptotically. The dominance of the two-body correlations is explained by the short-range healing distance of nucleons in the nuclear medium upon scattering [14].

Lastly, we address the effectiveness of using a spherical mean field. Nuclei are observed to carry well-defined angular momentum. The eigenfunctions of the Schrodinger equation in a spherically symmetric potential are also eigenfunctions of the total angular momentum operator $\hat{J}$. Given that the residual interactions and the spin-orbit interaction are generally spherically symmetric, mix the configurations with good total angular momentum quantum number (J) to give states with good J. Therefore, in the nuclear shell model treatment of the nucleus as a closed system, the angular momentum conservation holds, and dynamics of the nuclei can be modeled effectively [14].

The nuclear shell model has an important place in nuclear theory, as it continues to prevail in illuminating the seemingly endless aspects of nuclear many-body systems. Witnessing successful models of the phenomenon becoming windows to the principles underlying the phenomenon is a beautiful experience.

2.1.2 Theoretical Framework

We reiterate some details from the previous section. In the zeroth approximation, the nuclei are treated as bound states of nucleons that move independently in a spherically symmetric field. We denoted the Hamiltonian in this approximation as $H_0 = \sum[T_i + U_i]$, which dictates the energies of single-particle states, that the nucleons then occupy. For the further refinement of the results obtained, the two-body residual interaction $V = \frac{1}{2}\sum_{i\neq j}\nu(ij)$ is incorporated and treated as a perturbation. In the phenomenological treatment of the nuclear shell model, given the above, the Hamiltonian is written as [14]:

$$H = \sum[T_i + U(i)] + \frac{1}{2}\sum_{i\neq j}\nu(ij), \tag{1}$$

where

$$H_0 = \sum[T_i + U(i)] = \sum h(i). \tag{2}$$

Let single-particle eigenstates $\Phi_\alpha(i)$ be the eigenstates of H_0. $\nu(ij)$ is diagonalized in the subspace of degeneracies of equation (2). Such degeneracies may arise due to the symmetries of the Hamiltonian equation (2). This is the first set of corrections applied to the single-particle energies [14].

The mean-field potential U_i is scalar and spherically symmetric. It has two components: $\sum \xi(r_i,\tau_{i3})$ and $\sum \zeta(r_i) l_i.s_i$. $\sum \xi(r_i,\tau_{i3})$ commonly called the central potential has no angular dependence. r_i represents the radial dependence and τ_{i3} points to different central potentials for protons and neutrons. $\sum \zeta(r_i) l_i.s_i$ represents the spin-orbit potential necessary to account for the observed shell structure. Therefore the Hamiltonian H_0 can be expressed as $H_0 = \sum[T_i + \xi(r_i,\tau_{i3}) + \zeta(r_i) l_i.s_i]$. The modified Hamiltonian H is given as $H = H_0 + V$ [14].

For many-particle configuration, the reduced matrix element of any one-body operator $\hat{O}$ can be decomposed into a sum over single-particle matrix elements as [17, 18]:

$$\langle I\alpha||O^{\sigma L}||I'\alpha'\rangle = \sum_{j\alpha j'\alpha'} c_1(l,j,I,\alpha,l',j',I',\alpha')\langle lj||O^{\sigma L}||l'j'\rangle. \tag{3}$$

Also, reduced transition densities are given as:

$$B(O^{\sigma L}; I\alpha \to I'\alpha') = \frac{1}{2J'+1}\langle I\alpha||O^{\sigma L}||I'\alpha'\rangle^2. \tag{4}$$

In equation (3) and (4), (σL) specify the multipolarity L and the intrinsic parity σ of the operator, (l, j) the orbital and $(I\alpha)$ the state for initial (primed) and final state with α specifying any additional quantum number. The coefficients c_1 are calculated from the amplitudes of the configurations composing the wave functions, by angular momentum recoupling and decoupling single particles from N-particle configurations making use of coefficients of fractional parentage (cfp), which maintain antisymmetrization (see [17] and references therein).

2.2 Theory of β decay

2.2.1 Foundations

The study of nuclear β decay has a long history [20]. This study contributed to major developments and discoveries concerning the foundations of physics [20]. Among the fruits of this investigation are the discovery of weak interaction and neutrinos [20], the parity-violating nature of the weak interactions [21], and electroweak unification [22–25]. Such developments led to the characterization of weak interaction at low energies as of vector-axial vector (V-A) type. Investigations into nuclear β decay continue to inform foundational open questions. Some of these questions concern the determination of the properties of neutrinos [1], searches of dark matter [6, 7], and testing of fundamental symmetries [1–3]. Therefore, experimental and theoretical studies of nuclear β decay, remain relevant and deeply involved for searches of Beyond Standard Model Physics (BSMP).

There are three basic β decay processes, namely, β^-, β^+, and electron-capture (EC), of which electron-capture will be the focus of the study undertaken in this work. The three processes are depicted below [13]:

β^-decay:

$$n \rightarrow p + e^- + \bar{\nu_e}. \tag{5}$$

β^+decay:

$$p \rightarrow n + e^+ + \nu_e. \tag{6}$$

Electron-capture (EC) decay:

$$p + e^- \rightarrow n + \nu_e. \tag{7}$$

The conservation of momentum, energy, charge, leptons, and baryons are known to hold for these processes. Hence, the dynamics of these nuclear processes are dictated by the symmetries associated with these conservation laws [13].

These processes are mediated by the exchange of $W^{\pm}$ bosons of the weak interaction, and involve the creation and annihilation of particles/fields. Hence, the framework of field theory and the method of second quantization offers the best-known fundamental description for such processes [13, 20, 26]. Depending on the angular momentum and parity change involved in the β decay, β decay can be

classified into different categories.

These categories are allowed Fermi, allowed Gamow-Teller (GT), forbidden unique, and forbidden non-unique. The angular momentum and parity selection rules for these categories are given in tables 1-3, as per [13].

Table 1. Selection rules for allowed decays

Type of transition	$\Delta J = \lvert J_f - J_i \rvert$	$\pi_i \pi_f$
Fermi	0	+1
Gamow–Teller	1 ($J_i = 0$ or $J_f = 0$)	+1
Gamow–Teller	0, 1 ($J_i > 0$, $J_f > 0$)	+1

Table 2. Selection rules for forbidden unique transitions

K	1	2	3	4	5	6
ΔJ	2	3	4	5	6	7
$\pi_i \pi_f$	-1	$+1$	-1	$+1$	-1	$+1$

Table 3. Selection rules for forbidden non-unique transitions

K	1	2	3	4	5	6
ΔJ	0,1	2	3	4	5	6
$\pi_i \pi_f$	-1	+1	-1	+1	-1	+1

The process being semi-leptonic, involves both leptons and hadrons. The field theoretic level of analysis is apt for fields of point particles including leptons, quarks, and bosons that are considered fundamental in the treatment [20]. Since hadrons are not point particles but are composed of quarks, the transition from quark picture to hadron picture involves deriving hadronic currents from quark currents. This leads to a theory of nuclear β decay being formulated on the nucleonic level. A concise description of the movement from quark level to hadron level is given in [27]. The short range of $W^{\pm}$ bosons makes it reasonable to treat the weak interaction between leptons and hadrons as a point interaction. The interaction, as mentioned earlier is assumed to be of V-A type. The vector coupling g_V takes the value 1 at

both the quark level and hadronic level of analysis, at zero momentum exchange limit. On the other hand, axial-vector coupling g_A=1 is renormalized due to the effects of the strong interaction, to 1.276 (bare value: deduced from the free neutron decay) [28] at the hadronic level. Such scaling in the case of g_V and g_A are based on conserved vector current (CVC) and partially conserved axial vector current (PCAC) hypothesis resp. [14, 20, 26].

As one moves to a nucleon-level analysis of nuclear β decay, one enters the domain of nuclear phenomenology. As mentioned earlier, the β decay process is aptly treated as a point interaction between the hadronic and the leptonic currents. Therefore, on the nucleon level, the process is viewed to proceed as an interaction between nuclear-many body wave functions of the initial (wave function of the parent nucleus) and final (wave function of the daughter nucleus) states. The additional complexity of nuclear many-body correlations must be incorporated in modeling nuclear β decay. To this end, impulse approximation serves as a good first-order approximation [13, 29].

Nuclear phenomenology emerges as an attempt to deduce the physics of nuclear structure in the face of the nuclear many-body problem [30]. On the level of practice, this translates to computations of wave functions containing physics using different approximation schemes. Different approximation schemes correspond to different phenomenological nuclear models, where the richness of nuclear phenomenology reflects the challenge of solving the nuclear many-body problem exactly.

Multiple phenomenological treatments of nuclear dynamics exist, due to the lack of a unified and complete treatment of the dynamics of nuclear structures and processes. Different sets of implicit and explicit assumptions validate different phenomenological treatments. Therefore, clarity of such assumptions is needed to carefully interpret the physics of the process depending on the models. It is thus necessary to separate the model-dependent aspects and model-independent aspects. The theory of β decay was reformulated due to such need to separate model-dependent and model-independent aspects. This reformulation where model-dependent and model-independent aspects of physics could be separated, is the most accurate and useful version of the theory of β decay present to date [29, 31–33]. Some key details of this theory concerning the present work are outlined in the next section.

2.2.2 Theoretical Framework: Non-relativistic treatment of the theory of β decay

The reformulation of the theory of β decay alluded in the previous section is due to W. Bühring, B. Stech, and L. Schülke [31–33]. This framework based on impulse approximation made possible the clear and separate treatment of the kinematical structure, electromagnetic interaction, and model-dependent nuclear effects [26, 29]. Therefore, a harmonious treatment of the relationship between nuclear observables i.e. nuclear form factors and theoretically predicted nuclear matrix elements (NMEs), became possible. This relation between nuclear form factors and NMEs is possible for low-momentum transfer in impulse approximation [29].

Here we present key relations concerning electron-capture decays. Detailed treatment of the non-relativistic limit of the theory of β decays is well established and a detailed account is presented in [29]. A more concise and practical exposition of the treatment of forbidden β^+/EC decays is given in [34]. The half-life for β decay is given as:

$$t_{1/2} = \frac{\kappa}{\tilde{C}}, \tag{8}$$

where κ has the value of 6289 s. $\tilde{C}$ is the dimensionless integrated shape function. For allowed Gamow-Teller decays, $\tilde{C}$ takes the form:

$$\tilde{C} = f_0 C_{\mathrm{GT}}(w_e), \tag{9}$$

where f_0 is the phase-space factor, $C_{\mathrm{GT}}(w_e)$ the shape factor for Gamow-Teller decays. $C_{\mathrm{GT}}(w_e)$ is given as

$$C_{\mathrm{GT}}(w_e) = B_{\mathrm{GT}} \equiv \frac{g_{\mathrm{A}}^2}{2J_i + 1} |\mathcal{M}_{\mathrm{GT}}|^2. \tag{10}$$

$C_{\mathrm{GT}}(w_e)$ is commonly denoted as B_{GT} (reduced Gamow-Teller probability). $\mathcal{M}_{\mathrm{GT}}$ is the Gamow-Teller NME, J_i the nuclear spin of the initial state. $\mathrm{g_A}$ is the axial vector coupling.
$\tilde{C}$ for forbidden electron-capture decays take the form:

$$\tilde{C}^{\mathrm{EC}} = \frac{\pi}{2} \sum_{x=1s,2s} n_x \beta_x^2 (p_{\nu_x}/m_e c)^2 C(p_{\nu_x}) \,, \tag{11}$$

when considering the leading channels, namely K capture (1s) and $\mathrm{L_1}$ capture (2s).

Here n_x are relative occupancies for the respective orbitals, β_x are the electron Coulomb amplitudes, and p_{ν_x} is the momentum of the neutrino when the electron is captured from the atomic orbital x [34]. The shape factor $C(p_{\nu_x})$ used in equation (11), containing complicated combinations of phase-space factors and nuclear matrix elements (NMEs), is given for forbidden electron-capture transitions in detail in [34].

When a nucleus/nuclear state can decay via multiple branches, the branching ratio % (BR %) for a given branch is defined as:

$$\mathrm{BR}\% = \frac{\mathrm{t}_{1/2}^{\mathrm{tot}}}{\mathrm{t}_{1/2}} \times 100, \tag{12}$$

where $t_{1/2}$ is the partial half-life of the decay branch and $t_{1/2}^{\mathrm{tot}}$ is the total half-life of the decay.

2.3 Free parameters in predicting/reproducing experimental branching ratios and half-lives: $\mathrm{g}_{\mathrm{A}}^{\mathrm{eff}}$ and s-NME

Theoretical prediction of branching ratio/partial half-life depends on $\mathrm{g_A}$ due $\mathrm{g_A}$ dependence of $\tilde{C}$ of equation (8) for all β decays. As mentioned in the previous section, one works with approximate wave functions due to the difficulty of solving the nuclear many-body problem exactly [30].

It is seen that using the bare value of $\mathrm{g_A}$ with imperfect NMEs fails to reproduce experimental branching ratios (and spectral shapes in case of forbidden non-unique β^-decays [35, 36]). The problem of reproducing experimental branching ratio (and β^- spectral shapes) can and is solved using effective/quenched value of $\mathrm{g_A}$ i.e $\mathrm{g}_{\mathrm{A}}^{\mathrm{eff}}$ [27, 35–37]. Therefore, $\mathrm{g}_{\mathrm{A}}^{\mathrm{eff}}$ is treated as a free parameter for all weak interaction nuclear processes including β decay, as $\mathrm{g}_{\mathrm{A}}^{\mathrm{eff}}$ is an artifact of the incompleteness of the wave functions involved [38].

$\mathrm{g}_{\mathrm{A}}^{\mathrm{eff}}$ is related to the quenching factor q as [27]:

$$q = g_{\mathrm{A}}^{\mathrm{eff}}/g_{\mathrm{A}}, \tag{13}$$

where $\mathrm{g_A}$ is 1.276 [28]. The key inference we consider here is that for different branches of the decaying parent nucleus, q is not unique. This follows from the fact that not all wave functions are modeled well to the same degree in nuclear structure calculations. Justification of this inference is also evident from the evaluation of $\mathrm{g}_{\mathrm{A}}^{\mathrm{eff}}$

for similar allowed Gamow-Teller branches in the electron-capture decay of ^{57}Co, as can be seen in section 3.2. More completely modeled the states involved in the weak interaction nuclear process are, closer the the value of q is to 1 [38].

Since the experimental branching ratios are not known for the GS-to-GS transitions we are concerned with (see sections 1 and 3.3), therefore, theoretical branching ratios and $t_{1/2}$ are calculated for $g_A^{\text{eff}} \in$[0.5-1.27]. The range of g_A^{eff} is chosen so since for reasonably fit wave functions, the g_A^{eff} appears to be in this range [27, 35–37]. The fitness of the wave functions is indicated by the good agreement between the theoretical and experimental EM moments, which is the case for states involved in GS-to-GS transitions (see section 3.1).

For forbidden non-unique decays, NME contributions from beyond the active shell become necessary for such decays to be modeled reasonably [35, 36, 39]. The relativistic vector type NME ${}^{V}\mathcal{M}^{(0)}_{KK-11}$ incorporates such contributions. In perfect nuclear theoretical treatment, ${}^{V}\mathcal{M}^{(0)}_{KK-11}$ is related to non-relativistic vector large NME ${}^{V}\mathcal{M}^{(0)}_{KK0}$ as [29]:

$$ {}^{V}\mathcal{M}^{(0)}_{KK-11} = \left(\frac{\frac{(-m_n c^2 + m_p c^2 + W_0)R}{\hbar c} + \frac{6}{5}\alpha Z}{\sqrt{(K(2K+1))R}} \right) {}^{V}\mathcal{M}^{(0)}_{KK0}. \tag{14} $$

Here R is the nuclear radius and the other symbols represent the usual physical constants. We denote ${}^{V}\mathcal{M}^{(0)}_{KK-11}$ as small NME (s-NME). Equation (14) gives the CVC value of s-NME denoted as s-NME$_{\text{CVC}}$ [35, 36, 39]. Due to the lack of perfectly modeled wave functions, s-NME$_{\text{CVC}}$ falls short of reproducing experimental values of branching ratios [35, 36, 39].

In the absence of perfect nuclear theory, s-NME can be treated as a free parameter [39]. For each g_A^{eff}, varying s-NME predicts a range of branching ratios. Generally, when for a given g_A^{eff}, s-NME is fitted to experimental branching ratios/partial half-lives, it is seen that there exist two values of s-NMEs that reproduce branching ratios [36, 40–42]. It is the quadratic dependence of integrated shape factor $\tilde{C}$ on s-NME, that leads to the existence of two solutions. In the absence of the experimentally known branching ratio (as in the case of GS-to-GS transitions in this work), one needs to fix s-NME in a physically relevant way. It is seen that, for the dependence of $\tilde{C}$ on s-NME, there exists a unique s-NME that maximizes (partial) half-life ($t_{1/2}$) and in turn minimizes the branching ratio for the wave functions in use. This s-NME is denoted by s-NME$_{\text{min}}$ and gives way to predict the theoretical lower limit

of branching ratio i.e. BR_{min}. These aspects of forbidden non-unique decays are discussed further in section 3.2, in the context of the evaluation of the 1^{st}-forbidden non-unique known branch $^{44}Ti(0_1^+) \rightarrow ^{44}Sc^*(1_1^-)$.

3 Details of Calculations and Results

3.1 Nuclear Structure Calculations: NMEs and Electromagnetic observables

Nuclear wave functions for NME and electromagnetic (EM) observables are calculated using NuShellX@MSU [43]. ^{44}Ti and ^{44}Sc are computed in the SDPFPN-model space with NOWPN interaction with a ^{36}Ar core. ^{57}Co is computed using FPPN model space and GX1APN interaction. For ^{57}Fe, KB3GPN interaction is used in the FPPN model space with the truncation scheme of [44].

Table 4. Experimental and theoretical values of energies and EM moments of the states involved in electron-capture decay of the three sources. Energies in MeV, The magnetic dipole (μ), and electric quadrupole (Q) moments are given in units of nuclear magnetons (μ_N/c) and ebarns resp. In the calculations, an effective charge $1.5e$ ($0.5e$) for proton (neutron) and bare g factors were used [13]. Experimental values taken from [45].

Nucleus	J^π	E_{exp}	E_{theo}	μ_{exp}	μ_{theo}	Q_{exp}	Q_{theo}
$^{44}_{22}Ti_{22}$	0^+_1	0	0	-	-	-	-
$^{44}_{21}Sc_{23}$	2^+_1	0	0	+2.498(5)	+2.605	+0.10(5)	+0.0806
	1^-_1	0.068	7.410	+0.342(6)	-1.287	+0.21(2)	+0.0750
	0^-_1	0.146	9.093	-	-	-	-
$^{57}_{27}Co_{30}$	$7/2^-_1$	0	0	+4.720(10)	+4.568	+0.54(10)	+0.3876
$^{57}_{26}Fe_{31}$	$1/2^-_1$	0	0	+0.09064(7)	+0.130	-	0.00
	$3/2^-_1$	0.0144	0.022	-0.15531(18)	-0.387	+0.160(8)	+0.1726
	$5/2^-_1$	0.136	0.063	+0.935(10)	+0.980	-	-0.3173
	$5/2^-_2$	0.706	0.820	-	+0.533	-	-0.0533
$^{139}_{58}Ce_{81}$	$3/2^+_1$	0	0	+1.06(4)	+1.316	-	+0.2523
$^{139}_{57}La_{82}$	$7/2^+_1$	0	0	+2.7791(2)	+1.756	+0.206(4)	+0.1267
	$5/2^+_1$	0.166	0.082	-	+4.668	-	-0.1698

For ^{139}La and ^{139}Ce, JJ55PN model space is used with SN100PN interaction. 4

protons are fixed in $1g_{7/2}$ orbital for ^{139}Ce. Experimental and theoretical values of energies, magnetic dipole moment (μ), and electric quadrupole moment (Q) of states involved for all electron-capture decays are given in table 4.

Except for excited states in ^{44}Sc, theoretical energies of states involved in electron-capture decays are modeled well, as evident from results presented in table 4. The 1^-_1 and 0^-_1 states in ^{44}Sc arise due to the nucleon excitation from SD-shell to PF-shell. Moreover, the low experimental excitation energy for these states indicates that these states have a collective character. Therefore, for these states to be modeled reasonably, at the very least, full-scale calculation in the SDPFPN-model space would be required. Such heavy computation was not feasible given the limited computational resources. So a constrained calculation was done with ^{36}Ar core that can generate these excited states but does not perfectly model them. The theoretically predicted state has very high energies likely due to being modeled as single particle excitation across shells. Yet, these states suffice the purpose of informing our methodology for branching ratio estimation.

Table 5. Reduced transition probabilities in Weisskopf units (W.u.) for the magnetic dipole (M1) and electric quadrupole (E2) transitions, and their mixing ratios δ, for the transitions accompanying the axionic de-excitation under consideration. The used effective charges and g factors are those listed in table 4. Experimental values are taken from [45].

transition	M1	E2	δ
^{44}Sc$[0^-_1 \to 1^-_1]$			
Theory	0.01752	0.00000	0.00000
Experiment	$8.71(5)\times10^{-7}$	-	-
^{57}Fe$[3/2^-_1 \to 1/2^-_1]$			
Theory	0.03545	0.49	0.00183
Experiment	0.0078(3)	0.37(7)	0.00223(18)
^{139}La$[5/2^+_1 \to 7/2^+_1]$			
Theory	0.0001795	0.04414	0.052
Experiment	0.00257(4)	-	-

The magnetic dipole (μ) and electric quadrupole (Q) moments serve as primary markers of the fitness of the wave functions obtained from calculations. These

markers give information about how well modeled the wave functions are. This in turn informs our expectations, of the degree of quenching of g_A, for the electron-capture decay involving these states as discussed in section 2.3. It can be seen in table 4, that wave functions of the concerning nuclear states are fit, again except the excited states of ^{44}Sc, as indicated by the good agreement between theoretical and experimental values of EM moments (especially μ).

The decay of certain M1 decaying states is the potential source of low-mass axions as discussed in section 1. In table 5, transition strengths and mixing ratios of M1 decays concerning low-mass axion production in ^{44}Sc, ^{57}Fe, and ^{139}La are given.

3.2 Evaluation of known branches: Electron-capture decays of ^{44}Ti, ^{57}Co, and ^{139}Ce

Now, we discuss the evaluation of the known electron-capture branches in a theme, that informs the main focus of this work i.e. evaluation of the unknown GS-to-GS electron-capture branches (presented in the next section).

Figure 1. Electron-capture decay of ^{57}Co [46]

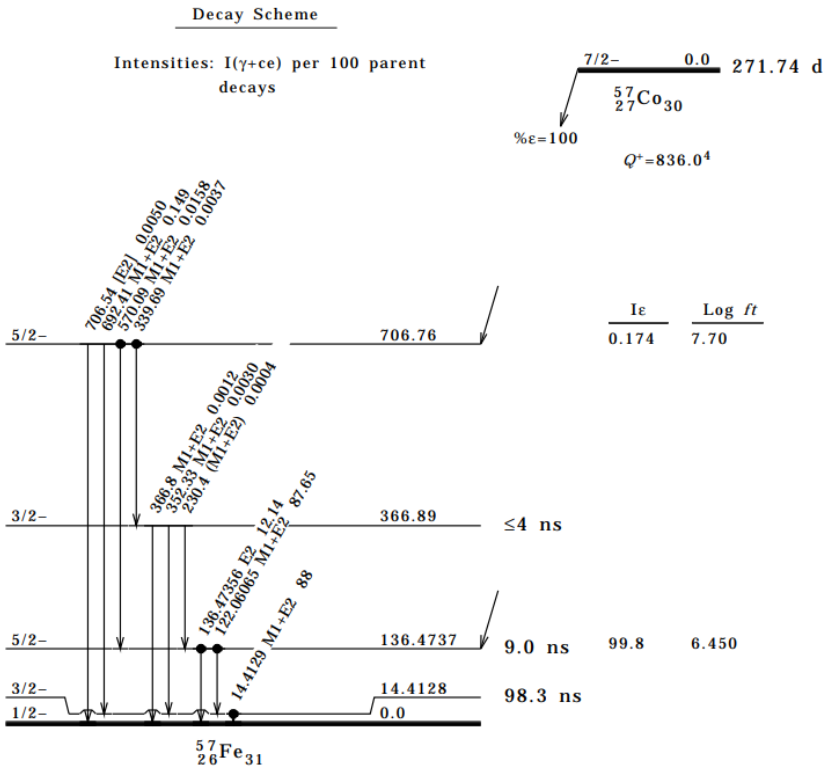

Starting with the electron-capture decay of ^{57}Co, the electron-capture decay scheme is given in figure 1.

The two known branches are Gamow-Teller decays that populate the $5/2_1^-$ and $5/2_2^-$ levels in ^{57}Fe with branching ratios of 99.8(3) % and 0.174(10) % resp. [45].

The branches are identical as the initial and final J^π are the same. Also, the wave functions of the initial state are common for both. The g_A^{eff} for these resp. branches are 1.2524 and 0.5477 for M_{GT} -0.1065 and 0.0572 resp., using the phase-space factors of [47]. This difference in quenching is due to the difference in the quality of the final state wave functions. Table 4 shows that for $5/2_1^-$ state, μ is in very good agreement with the experimental value, justifying a large q value of 0.982. Hence the inference of non-uniqueness of the g_A^{eff} stated in section 2.3 is evident when we look at the two Gamow-Teller branches of the decay of ^{57}Co.

In the decay of ^{139}Ce (see figure 2), the only known branch is the Gamow-Teller decay populating the $5/2_1^+$ state with BR≈100% [45] turns out to have g_A^{eff}=0.91376 for M_{GT}=0.3403 using the phase-space factors of [47].

Figure 2. Electron-capture decay of ^{139}Ce [48]

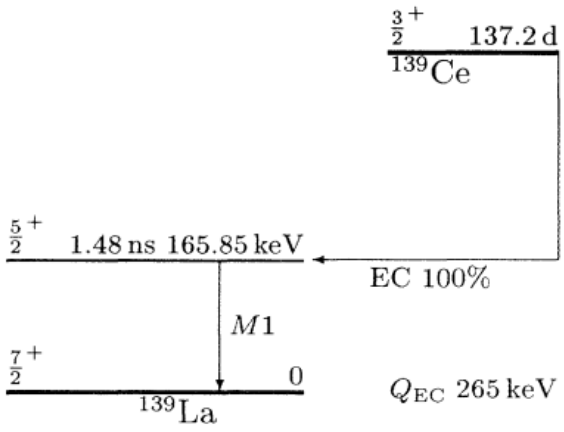

Lastly, the electron-capture decay of ^{44}Ti is depicted in figure 3. Multiple measurements of branching ratios for electron-capture decay of ^{44}Ti have been made. One such measurement is shown in figure 3.

We use the experimental values of branching ratios provided in [49]. We use these values since the uncertainty is minimum for measurements in [49]. According to [49], decay of 0_1^+ GS of ^{44}Ti is known to populate excited states 1_1^- and 0_1^- in ^{44}Sc with experimental branching ratio 0.7(3)% and 99.3(3)% resp.

Figure 3. Electron-capture decay of ^{44}Ti [50]

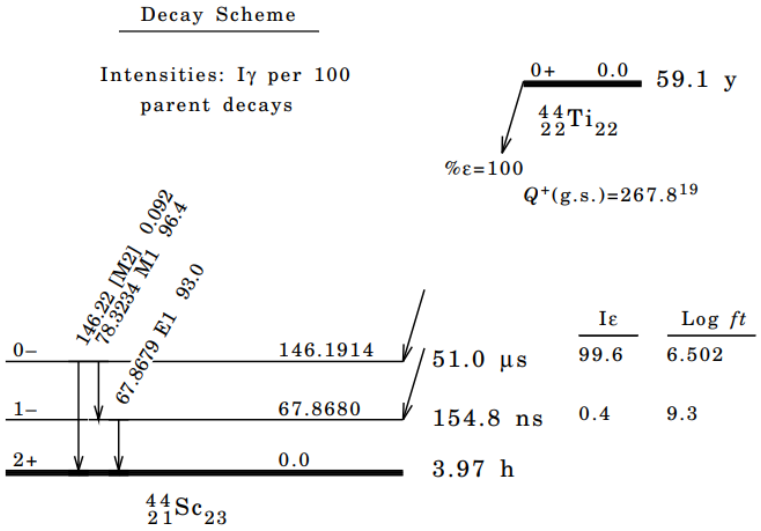

Both these branches are 1st-forbidden non-unique. The forbidden non-unique branch populating 0_1^- is independent of s-NME value, therefore we skip the evaluation of this branch. Evaluating the ^{44}Ti$(0_1^+) \rightarrow ^{44}$Sc*$(1_1^-)$ branch will help demonstrate the location of s-NME that minimizes the theoretical branching ratio (s-NME$_{\rm min}$) w.r.t the two s-NMEs that reproduce experimental branching ratio (s-NME$_1$/s-NME$_2$).

Table 6. Computed s-NME values (s-NME$_1$ and s-NME$_2$) which reproduce the experimental BR of the ^{44}Ti$(0_1^+) \rightarrow ^{44}$Sc*$(1_1^-)$ transition and the s-NME value s-NME$_{\rm min}$ which minimizes the BR of this transition for the effective weak axial couplings of interest in this work. The CVC value of the s-NME, s-NME$_{\rm CVC}$, is given for reference.

$g_A^{\rm eff}$	s-NME$_1$,s-NME$_2$	s-NME$_{\rm min}$
0.5	-0.005349275, -0.0009363725	-0.00314283,
0.6	-0.0059552,-0.00154135	-0.00374827
0.7	-0.006561075, -0.002146375	-0.00435373
0.8	-0.007166905, -0.002751445	-0.00495918
0.9	-0.007772685, -0.003356565	-0.00556462
1.0	-0.00837842, -0.003961729	-0.00617007
1.1	-0.00898411, -0.004566938	-0.00677552
1.2	-0.00958975, -0.005172195	-0.00738098
1.27	-0.010013675, -0.005595905	-0.00780479
	s-NME$_{\rm CVC}$:-0.0134970658	

To this end, the results of the evaluation are presented in table 6 for $g_A^{eff} \in$[0.5-1.27].

The variation of theoretical branching ratio with s-NME value is presented in figure 4 to demonstrate the location of branching ratio minima corresponding to s-NME_{min} and the location of s-NME_1/s-NME_2 (intersection of branching ratio curves with the horizontal line of BR_{exp}). In figure 4, it can be seen that s-NME_{min} is located in between the two s-$NME_{1/2}$ values.

Figure 4. The variation of theoretical branching ratio with s-NME for $^{44}Ti(0_1^+) \rightarrow ^{44}Sc^*(1_1^-)$ transition. For $g_A^{eff} \in$[0.5-1.27], branching ratio minima corresponds to s-NME_{min}. The locations of s-NME_1 and s-NME_2 are the intersection points of branching ratio curves with the horizontal line corresponding to BR_{exp}.

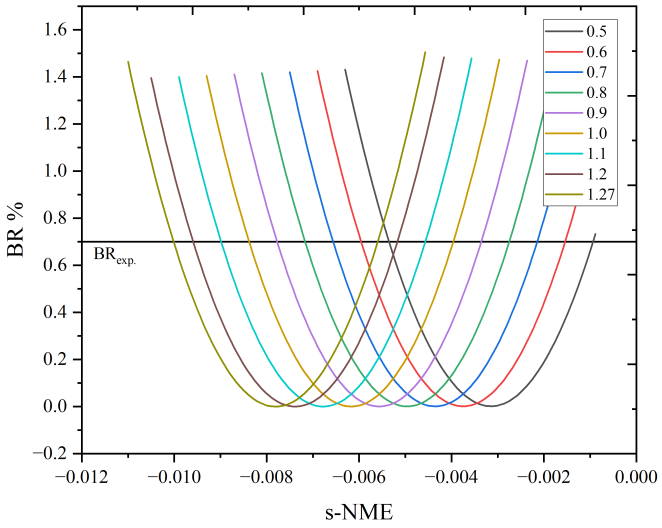

That is s-NME values more or less than s-NME_{min} produce larger branchings, for all g_A^{eff}. The s-NME_{CVC} fails to reproduce experimental branching ratio with reasonable g_A^{eff} in case of 1st-forbidden non-unique we evaluated, and reproduces the experimental branching ratio for g_A^{eff}>1.276.

3.3 Evaluation of unknown GS-to-GS branches: Electron-capture decays of ^{44}Ti, ^{57}Co, and ^{139}Ce

As already mentioned in section 3.1, the ground states are modeled well as seen from the good agreement between theoretical and experimental values of EM moments presented in table 4. Following the discussion of section 2.3, in table 7, the evaluated theoretical minimum branching ratio (BR_{min}), maximum partial half-lives ($t_{1/2,max}$) and the corresponding s-NME_{min} are tabulated for the 2nd-forbidden non-unique decays of ^{44}Ti and ^{139}Ce. Also, presented are the theoretical branching ratios (BR) and partial half-lives ($t_{1/2}$) for the 2nd-forbidden unique decay of ^{57}Co.

Table 7. Values of s-NMEs (s-NME_{min}) which minimize the theoretical branching ratio (BR_{min}) and hence maximize the corresponding partial half-life ($t_{1/2,max}$) for the effective weak axial couplings of interest in this work. The transition $^{57}Co(7/2^-_1) \rightarrow {}^{57}Fe(1/2^-_1)$ is forbidden unique and thus independent of s-NME. The lowest values of the branching ratio are highlighted, and they can serve as conservative estimates for experiments. The CVC value of the s-NME, s-NME_{CVC}, is given for reference.

	$^{44}Ti(0^+_1) \rightarrow {}^{44}Sc(2^+_1)$ 2ndforb.non-unique			$^{57}Co(7/2^-_1) \rightarrow {}^{57}Fe(1/2^-_1)$ 2ndforb.unique		$^{139}Ce(3/2^+_1) \rightarrow {}^{139}La(7/2^+_1)$ 2nd forb.non-unique		
g_A^{eff}	s-NME_{min}	BR_{min}[%]	$t_{1/2,max}$[s]	BR[%]	$t_{1/2}$[s]	s-NME_{min}	BR_{min}[%]	$t_{1/2,max}$[s]
0.5	-0.0203432	6.15039E-7	3.03235E+17	**1.62975E-7**	1.44061E+16	-0.135510	**9.9991E-8**	1.18923E+16
0.6	-0.0237749	5.9534E-7	3.13269E+17	2.34685E-7	1.00042E+16	-0.16324	1.11886E-7	1.0628E+16
0.7	-0.0272068	5.75961E-7	3.23809E+17	3.19431E-7	7.35005E+15	-0.190975	1.24612E-7	9.54258E+15
0.8	-0.030640	5.56905E-7	3.34889E+17	4.17216E-7	5.62738E+15	-0.21871	1.38171E-7	8.60615E+15
0.9	-0.034070	5.38168E-7	3.46549E+17	5.28039E-7	4.44633E+15	-0.24644	1.52563E-7	7.79433E+15
1.0	-0.037501	5.19752E-7	3.58828E+17	6.51901E-7	3.60152E+15	-0.274178	1.67786E-7	7.08715E+15
1.1	-0.040934	5.01657E-7	3.71771E+17	7.88798E-7	2.97647E+15	-0.301912	1.83841E-7	6.4682E+15
1.2	-0.044365	4.83881E-7	3.85428E+17	9.38735E-7	2.50106E+15	-0.329645	2.00729E-7	5.92401E+15
1.27	-0.046767	**4.7163E-7**	3.9544E+17	1.05145E-6	2.23295E+15	-0.349058	2.13046E-7	5.58153E+15
	s-NME_{CVC}:-0.230519384					s-NME_{CVC}:0.397514939		

The BR_{min} values for forbidden non-unique decays are quite stable with the variation of g_A^{eff}, as can be seen in figure 5. The branching ratio for forbidden unique decay varies more quickly with g_A^{eff}, given that g_A^{eff} is the only free parameter for forbidden unique decays.

Figure 5. Variation of branching ratio estimates with g_A^{eff} for 2^{nd}-forbidden non-unique (left panel) and 2^{nd}-forbidden unique (right panel) GS-to-GS transitions

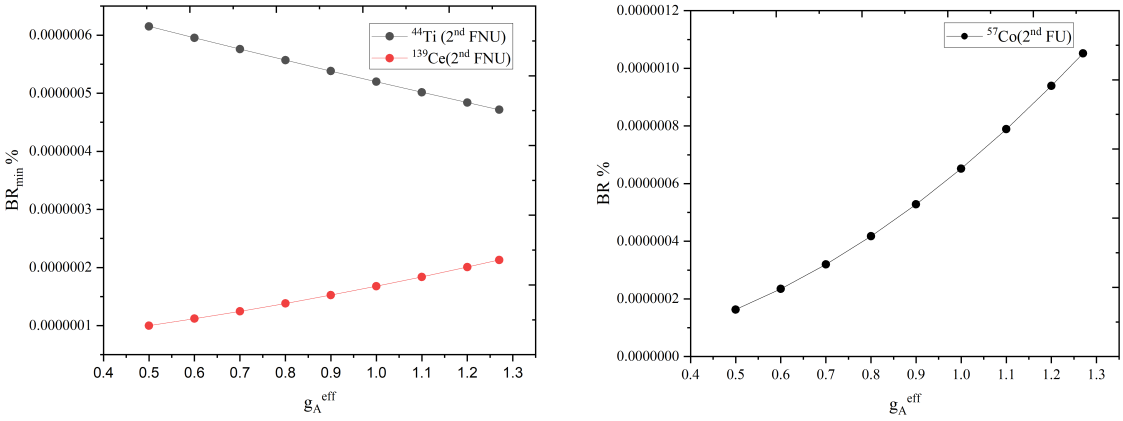

The most conservative estimate for the given GS-to-GS transition is the lowest branching ratio obtained for the g_A^{eff} range under consideration. This value is suggested for the experiments. In the case of the 2^{nd}-forbidden non-unique GS-to-GS branch of ^{139}Ce, the upper limit of experimental branching ratio was established to be $5(5)\times10^{-7}$ % [6]. Our BR_{min} estimates of this decay are compatible with the experimental upper limit.

4 Conclusion and Outlook

To summarize, the advanced theory of β decay is used to make predictions for the transition rates, of unknown GS-to-GS electron-capture decay of ^{44}Ti, ^{57}Co, and ^{139}Ce. The decays include 2^{nd}- forbidden non-unique transitions in ^{44}Ti and ^{139}Ce, along with 2^{nd}-forbidden unique transition in ^{57}Co. These decays concern the experimental searches of low-mass axions. A new strategy is formulated in this work to give predictions for these unknown electron-capture branches.

The theory predictions are compatible with the presently limited experimental information for GS-to-GS transitions. The conservative estimates of minimum theoretical branching ratios (rounded to two decimal places here) are 4.72×10^{-7} % for the decay of ^{44}Ti, 1.63×10^{-7} % for the decay of ^{57}Co, and 1.00×10^{-7} % for the decay of ^{139}Ce.

Due to the lack of experimental branching ratio measurements for these GS-to-GS branches, the theory predictions presented are expected to be useful for experimental searches of low-mass axions. In bringing the aim of this work to fruition, new aspects of $g_{\text{A}}^{\text{eff}}$ and s-NME evaluations come to light. This work also sets the precedence for β decay studies for other avenues of BSMP searches using β decays.

References

[1] H. Ejiri, J. Suhonen, and K. Zuber. "Neutrino–nuclear responses for astro-neutrinos, single beta decays and double beta decays". In: *Physics Reports* 797 (2019), pp. 1–102. DOI: https://doi.org/10.1016/j.physrep.2018.12.001.

[2] M. Brodeur et al. "Nuclear β decay as a probe for physics beyond the Standard Model". In: (2023). arXiv: 2301.03975 [nucl-ex].

[3] M. González-Alonso, O. Naviliat-Cuncic, and N. Severijns. "New physics searches in nuclear and neutron β decay". In: *Progress in Particle and Nuclear Physics* 104 (2019), pp. 165–223. DOI: https://doi.org/10.1016/j.ppnp.2018.08.002.

[4] V. Guadilla et al. "First measurements with a new β-electron detector for spectral shape studies". In: *Journal of Instrumentation* 19.02 (2024), P02027. DOI: 10.1088/1748-0221/19/02/P02027.

[5] L. Pagnanini et al. "Array of cryogenic calorimeters to evaluate the spectral shape of forbidden β-decays: the ACCESS project." In: *Eur. Phys. J. Plus* 138,445 (2023). DOI: https://doi.org/10.1140/epjp/s13360-023-03946-x.

[6] M. Minowa et al. "Invisible axion search in ^{139}La M1 transition". In: *Phys. Rev. Lett.* 71 (1993), pp. 4120–4123. DOI: 10.1103/PhysRevLett.71.4120.

[7] R. Massarczyk, P.-H. Chu, and S. R. Elliott. "Axion emission from nuclear magnetic dipole transitions". In: *Phys. Rev. D* 105 (2022), p. 015031. DOI: 10.1103/PhysRevD.105.015031.

[8] R. D. Peccei and H. R. Quinn. "CP Conservation in the Presence of Pseudoparticles". In: *Phys. Rev. Lett.* 38 (1977), pp. 1440–1443. DOI: 10.1103/PhysRevLett.38.1440.

[9] S. Weinberg. "A New Light Boson?" In: *Phys. Rev. Lett.* 40 (1978), pp. 223–226. DOI: 10.1103/PhysRevLett.40.223.

[10] F. Wilczek. "Problem of Strong P and T Invariance in the Presence of Instantons". In: *Phys. Rev. Lett.* 40 (1978), pp. 279–282. DOI: 10.1103/PhysRevLett.40.279.

[11] I. G. Irastorza and J. Redondo. "New experimental approaches in the search for axion-like particles". In: *Progress in Particle and Nuclear Physics* 102 (2018), pp. 89–159. DOI: https://doi.org/10.1016/j.ppnp.2018.05.003.

[12] T. W. Donnelly et al. "Do axions exist?" In: *Phys. Rev. D* 18 (1978), pp. 1607–1620. DOI: 10.1103/PhysRevD.18.1607.

[13] J. Suhonen. *From Nucleons to Nucleus*. Springer Berlin, Heidelberg, 2007.

[14] A. deShalit and H. Feshbach. *Theoretical Nuclear Physics Volume 1: Nuclear Structure*. John Wiley Sons, 1974.

[15] G. Brown, J. Holt, and T. Kuo. *The Nucleon-nucleon Interaction and the Nuclear Many-body Problem: Selected Papers of Gerald E. Brown and T.T.S. Kuo*. World Scientific, 2010.

[16] H. S. Alexandre Obertelli. *Modern Nuclear Physics*. Springer Singapore, 2022.

[17] H. Grawe. "Shell Model from a Practitioner's Point of View". In: *The Euroschool Lectures on Physics with Exotic Beams, Vol. I*. Ed. by J. Al-Khalili and E. Roeckl. Springer Berlin Heidelberg, 2004, pp. 33–75. DOI: 10.1007/978-3-540-44490-9_2.

[18] A. deShalit and I. Talmi. *Nuclear Shell Theory*. Academic Press, 1963.

[19] I. Talmi. *Simple Models of Complex Nuclei*. CRC Press, 1993.

[20] M. S. Athar and S. K. Singh. *The Physics of Neutrino Interactions*. Cambridge University Press, 2020.

[21] C. S. Wu et al. "Experimental Test of Parity Conservation in Beta Decay". In: *Phys. Rev.* 105 (1957), pp. 1413–1415. DOI: 10.1103/PhysRev.105.1413.

[22] S. Weinberg. "A Model of Leptons". In: *Phys. Rev. Lett.* 19 (1967), pp. 1264–1266. DOI: 10.1103/PhysRevLett.19.1264.

[23] A. Salam. "On parity conservation and neutrino mass". In: *Il Nuovo Cimento (1955-1965)* 5 (1957), pp. 299–301. URL: https://api.semanticscholar.org/CorpusID:123090429.

[24] A. Salam. “Weak and Electromagnetic Interactions”. In: *Conf. Proc. C* 680519 (1968), pp. 367–377. DOI: 10.1142/9789812795915_0034.

[25] S. L. Glashow, J. Iliopoulos, and L. Maiani. “Weak Interactions with Lepton-Hadron Symmetry”. In: *Phys. Rev. D* 2 (1970), pp. 1285–1292. DOI: 10.1103/PhysRevD.2.1285.

[26] H. F. .Schopper. *Weak interactions and nuclear beta decay*. North-Holland Publishing Company, 1966.

[27] J. T. Suhonen. “Value of the Axial-Vector Coupling Strength in β and $\beta\beta$ Decays: A Review”. In: *Frontiers in Physics* 5 (2017). DOI: 10.3389/fphy.2017.00055.

[28] B. Märkisch et al. “Measurement of the Weak Axial-Vector Coupling Constant in the Decay of Free Neutrons Using a Pulsed Cold Neutron Beam”. In: *Phys. Rev. Lett.* 122 (2019), p. 242501. DOI: 10.1103/PhysRevLett.122.242501.

[29] H. O. Behrens and W. Bühring. *Electron radial wave functions and nuclear beta-decay*. Oxford University Press, 1982.

[30] P. Ring and P. Schuck. *The Nuclear Many-Body Problem*. Springer Berlin, Heidelberg, 1980.

[31] W. Bühring. “Beta decay theory using exact electron radial wave functions”. In: *Nucl.Phys.* 40 (1963), pp. 472–488. DOI: https://doi.org/10.1016/0029-5582(63)90290-6.

[32] W. Bühring. “Beta decay theory using exact electron radial wave functions (II)”. In: *Nucl.Phys.* 49 (1963), pp. 190–208. DOI: https://doi.org/10.1016/0029-5582(63)90086-5.

[33] B. Stech and L. Schülke. “Nuclear β-decay.I and II”. In: *Z.Phys.* 179 (1964), pp. 314–342.

[34] E. Ydrefors, M. Mustonen, and J. Suhonen. “MQPM description of the structure and beta decays of the odd A=95,97 Mo and Tc isotopes”. In: *Nuclear Physics A* 842.1 (2010), pp. 33–47. DOI: https://doi.org/10.1016/j.nuclphysa.2010.04.005.

[35] J. Kostensalo et al. "Confirmation of g_A quenching using the revised spectrum-shape method for the analysis of the ^{113}Cd β-decay as measured with the COBRA demonstrator". In: *Physics Letters B* 822 (2021), p. 136652. DOI: https://doi.org/10.1016/j.physletb.2021.136652.

[36] L. Pagnanini et al. *Simultaneous Measurement of Half-Life and Spectral Shape of ^{115}In β-decay with an Indium Iodide Cryogenic Calorimeter*. 2024. arXiv: 2401.16059 [nucl-ex].

[37] J. Suhonen and J. Kostensalo. "Double β Decay and the Axial Strength". In: *Frontiers in Physics* 7 (2019). DOI: 10.3389/fphy.2019.00029.

[38] P. Gysbers et al. "Discrepancy between experimental and theoretical β-decay rates resolved from first principles". In: *Nat. Phys.* 15 (2019), pp. 428–431. DOI: https://doi.org/10.1038/s41567-019-0450-7.

[39] A. Kumar et al. "Second-forbidden nonunique β^- decays of ^{24}Na and ^{36}Cl assessed by the nuclear shell model". In: *Phys. Rev. C* 101 (2020), p. 064304. DOI: 10.1103/PhysRevC.101.064304.

[40] J. Kostensalo et al. "^{113}Cd β-decay spectrum and g_A quenching using spectral moments". In: *Phys. Rev. C* 107 (2023), p. 055502. DOI: 10.1103/PhysRevC.107.055502.

[41] M. Ramalho and J. Suhonen. "Computed total β-electron spectra for decays of Pb and Bi in the ^{220,222}Rn radioactive chains". In: *Phys. Rev. C* 109 (2024), p. 014326. DOI: 10.1103/PhysRevC.109.014326.

[42] R. Marlom and S. Jouni. "g_A-sensitive β spectral shapes in the mass $A = 86-99$ region assessed by the nuclear shell model". In: *Phys. Rev. C* 109 (2024), p. 034321. DOI: 10.1103/PhysRevC.109.034321.

[43] B. Brown and W. Rae. "The Shell-Model Code NuShellX@MSU". In: *Nuclear Data Sheets* 120 (2014), pp. 115–118. ISSN: 0090-3752. DOI: https://doi.org/10.1016/j.nds.2014.07.022.

[44] F. A. III et al. "Estimating the flux of the 14.4 keV solar axions". In: *Journal of Cosmology and Astroparticle Physics* 2018.01 (2018), p. 021. DOI: 10.1088/1475-7516/2018/01/021.

[45] "ENSDF database". In: *National Nuclear Data Center (NNDC)* (2024). URL: https://www.nndc.bnl.gov/ensdf/.

[46] M. Bhat. "Nuclear Data Sheets for A = 57". In: *Nuclear Data Sheets* 85.3 (1998), pp. 415–536. DOI: https://doi.org/10.1006/ndsh.1998.0021.

[47] N. Gove and M. Martin. "Log-f tables for beta decay". In: *Atomic Data and Nuclear Data Tables* 10.3 (1971), pp. 205–219. DOI: https://doi.org/10.1016/S0092-640X(71)80026-8.

[48] C. M. L. Virginia S. Shirley Edgardo Browne. *Table of isotopes. 7th ed.* Wiley, New York, 1978.

[49] Alburger et al. "First-forbidden $0^+ \rightarrow 0^-, 1^-$ electron capture of ^{44}Ti". In: *Phys. Rev. C* 38 (1988), pp. 1843–1851. DOI: 10.1103/PhysRevC.38.1843.

[50] J. Chen, B. Singh, and J. A. Cameron. "Nuclear Data Sheets for A = 44". In: *Nuclear Data Sheets* 112.9 (2011), pp. 2357–2495. DOI: https://doi.org/10.1016/j.nds.2011.08.005.